Testing and Modeling of MR Damper and Its Application to SDOF Systems Using Integral Backstepping Technique

Sk. Faruque Ali
Research Scholar
e-mail: skfali@civil.iisc.ernet.in

Ananth Ramaswamy
Associate Professor
e-mail: ananth@civil.iisc.ernet.in

Department of Civil Engineering,
Indian Institute of Science,
Bangalore,
Karnataka 560012, India

Magnetorheological dampers are intrinsically nonlinear devices, which make the modeling and design of a suitable control algorithm an interesting and challenging task. To evaluate the potential of magnetorheological (MR) dampers in control applications and to take full advantages of its unique features, a mathematical model to accurately reproduce its dynamic behavior has to be developed and then a proper control strategy has to be taken that is implementable and can fully utilize their capabilities as a semi-active control device. The present paper focuses on both the aspects. First, the paper reports the testing of a magnetorheological damper with an universal testing machine, for a set of frequency, amplitude, and current. A modified Bouc–Wen model considering the amplitude and input current dependence of the damper parameters has been proposed. It has been shown that the damper response can be satisfactorily predicted with this model. Second, a backstepping based nonlinear current monitoring of magnetorheological dampers for semi-active control of structures under earthquakes has been developed. It provides a stable nonlinear magnetorheological damper current monitoring directly based on system feedback such that current change in magnetorheological damper is gradual. Unlike other MR damper control techniques available in literature, the main advantage of the proposed technique lies in its current input prediction directly based on system feedback and smooth update of input current. Furthermore, while developing the proposed semi-active algorithm, the dynamics of the supplied and commanded current to the damper has been considered. The efficiency of the proposed technique has been shown taking a base isolated three story building under a set of seismic excitation. Comparison with widely used clipped-optimal strategy has also been shown.
[DOI: 10.1115/1.3072154]

Keywords: stay cable vibration, structural control, fuzzy logic, genetic algorithms, dynamic inversion

1 Introduction

One of the biggest challenges structural engineers face today is finding more effective means for protecting structures and their contents from the damaging effects of dynamic hazards such as strong earthquakes. Destructive seismic events over centuries throughout the world have clearly demonstrated the importance and the urgency of mitigating the effect of such natural hazards on structures. The idea of using control systems to dissipate, counteract, or deflect vibration energy has been identified as one promising approach in this direction (see Refs. [1,2]).

A control system can be classified as either passive, active, hybrid, or semi-active based on the level of energy required and the type of devices employed. Among these systems, the semi-active approach has recently received considerable attention because it offers significant adaptability of active systems without large power requirements and is reliable as passive systems. Rapid-response, fail-safe, low power requirement, simple interfaces between electronic controls and mechanical systems [3] are some characteristics of magnetorheological (MR) devices that have attracted significant research interest for using them as semi-active control devices in applications of vibration mitigation [2,4–8]. In particular, it has been found that MR dampers can be

designed to be very effective vibration control actuators. In Civil Engineering, MR damper applications mainly centered around the structural vibration control under wind [8] or earthquake excitation [4,5]. The automotive industry has been interested in developing applications of these materials, for example, for engine mounts, shock absorbers, clutches, and seat dampers [6,9].

A MR damper consists of a hydraulic cylinder containing MR fluid that, in the presence of a magnetic field, can reversibly change from a free-flowing, linear viscous fluid to a semisolid with controllable yield strength in fraction of a second. A MR fluid is a suspension of micronsized magnetically soft particles in a carrier liquid (such as water, mineral, or synthetic oil) that exhibits dramatic changes in rheological properties. Under the influence of a magnetic field these particles arrange themselves to form very strong chains of "fluxes" [10,11]. Once aligned in this manner, the particles are restrained from moving away from their respective flux lines and act as a barrier preventing the flow of the carrier fluid. Additives are commonly added to discourage settling, improve lubricity, modify viscosity, and reduce wear.

The MR damper, however, is an intrinsically nonlinear device, which makes the modeling and design of suitable control algorithms an interesting and challenging task. To evaluate the potential of MR dampers in control applications and to take full advantages of its unique features, a mathematical model that accurately reproduces the dynamic behavior has to be developed through a suite of tests conducted using MR damper. To practically implement the device for real time vibration control one has to develop

a proper control algorithm to monitor the MR damper current online. In the present paper both the aspects have been considered. A RD-1005–3 MR damper manufactured by LORD® [12] has been tested under harmonic excitation with different amplitudes, frequencies, and current supplies. The Bouc–Wen model proposed by Spencer et al. [13] has been modified based on the experimental results and a current and amplitude dependent modified Bouc–Wen model has been formulated for development of control algorithm and its application.

Based on mechanisms, both nonparametric and parametric models have been reported in literature to describe the observed behaviors of electro-rheological (ER) and MR devices. Ehrgott and Masri [14] presented a nonparametric approach for modeling ER fluid dampers by assuming that the damper force could be written in terms of Chebyshev polynomials in the damper velocity and acceleration. One of the difficulties in this approach is that the resulting models are often quite complex. On the other hand parametric models are based on simple mechanical idealizations. Spencer et al. [13] proposed the Bouc–Wen model to describe MR damper behavior. Makris and Dargush [15] developed a phenomenological elastic-plastic model to account for the preyield and postyield behaviors. Kamath et al. [16,17] also developed an augmented six parameter model to simulate both the force-displacement and the force-velocity hysteresis cycles. None of the parameters take care of the amplitude and frequency dependence of the parameters. Recent studies by Refs. [10,18–21] have shown the necessity of an amplitude and frequency dependence parameter modeling. Yang et al. [10] and Dominguez et al. [21] reported an exponential function to model the dependence of the parameters on the amplitude and frequency of excitation.

A wide range of theoretical and experimental studies has been performed to assess the efficacy of MR dampers as semi-active devices. Among the developed control strategies mentioned may be made of "skyhook" damper control algorithm [9], bang-bang controller [22], Lyapunov direct method [23], homogeneous friction algorithm [24,25], and clipped-optimal [5].

The first application of MR dampers to protect Civil Engineering structures under seismic motions has been conducted by Sain and co-workers [5,13]. Dyke et al. [5] proposed a clipped-optimal control algorithm based on acceleration feedback for the MR damper. In this approach, a linear optimal controller, combined with a force feedback loop, was designed to adjust the command voltage (and therefore current) of the MR damper. The command signal was set at either zero or the maximum level depending on how the damper's force compared with the target optimal control force. The target optimal control can be the linear quadratic regulator (LQR) [1], the H_2/LQG [5], Lyapunov based methods [26], etc.

Magnetorheological dampers are nonlinear devices, whose damping is varied by changing the input current (or voltage) to the damper. This makes the choice and design of control algorithm a difficult task as the designer has to choose proper map from force predicted by the algorithm and the current/voltage input to the MR damper. Most algorithms including widely used clipped-optimal algorithm swap the voltage input to the MR damper between zero and maximum voltage allowed based on the prescribed force by the control algorithm and the force measured at the damper connection.

The main disadvantage of these control strategies is that they do not consider any intermediate voltage supply [27]. Therefore neither of them provides optimal force required by the system. It has been shown in Ref. [27] that sometimes this swift change in voltage (current) led to a sudden rise in the external control force, which increases system responses and may introduce local damages within the structure. Moreover, the clipped-optimal strategy needs the measurement of the force the damper provides. Here, the mathematical information regarding the structure is used for the calculation of control forces to compare with damper force, obtained experimentally. To realize these control forces, knowl-edge of the actuator's dynamics is frequently quite important. Command signals need to be calculated and sent to the actuator so that it can produce the commanded control force. When the relation between the command signals and the actuator forces is linear or can be explicitly established, the calculation of command signals is not an issue. If, however, the relation cannot be explicitly established, then it is likely that the command signals cannot be easily obtained beforehand and some feedback actions are needed to correct the actuator's forces. Therefore, there is a need for control algorithms, which can change the MR damper current (and therefore voltage) slowly and smoothly, such that all current values between maximum and zero currents can be covered, based on the feedback from the structure.

In this context various intelligent methods (neural controllers [28] and nonadaptive and adaptive fuzzy controllers [27]) have been tried where damper monitoring voltage (current) is directly set based on system feedback. Ali and Ramaswamy [27] provided a comparison of adaptive, nonadaptive, and Lyapunov based clipped-optimal strategies for a nonlinear based isolated benchmark building. Neither the intelligent controllers nor the model based clipped-optimal controllers consider the effect of the input current to commanded current dynamics (the current actually goes to the coil to create magnetic flux). The dynamics matters less when the supplied current is a constant and does not vary (passive control case). When the supplied current to the MR damper is varied based on the system responses and desired performance of the system, this supplied current and the commanded current play a crucial role.

In this paper apart from the reported experimental investigation on a MR damper, a control algorithm for the MR damper current monitoring based on integrator backstepping [29] has been proposed. The reported algorithm provides an optimal current input to the MR dampers without any measurement of damper force (unlike clipped-optimal strategies). Integrator backstepping based control algorithm provides current required by the damper directly from the system dynamics. This to the best of the author's knowledge has not been reported earlier in literature, where clipped-optimal strategies are reported mostly. Furthermore, the algorithm provides a smooth change in damper current considering the MR damper supplied current-commanded current dynamics. Since the algorithm provides an optimal current input to the MR damper, it is amenable for online applications.

The paper has been organized as follows. Section 2 gives details of RD-1005–3 MR damper experiment under displacement monitored harmonic excitation. Details of the test setup and experimental results have been discussed. In Sec. 3 details of the analytical modeling of MR damper hysteretic behavior have been projected. Amplitude and input current dependent modified Bouc–Wen model has been considered to fit the experimental results. Details of the nonlinear force-current relation needed for a nonlinear current monitoring for online applications have been outlined. Section 4 gives details of the development of a stable controller design based on integrator backstepping for MR damper current monitoring. Finally, numerical simulation of a base isolated three story building response has been shown. Various earthquake records have been considered for numerical simulation. Results are shown for one seismic ground motion and results obtained from other earthquake simulations have been tabulated. Impulsive force response of the uncontrolled and controlled system also has been shown.

2 Harmonic Testing of MR Damper

The schematic of a prototype MR damper (RD-1005–3), supplied by Lord® Corporation, is shown in Fig. 1(a). This can be applied to an adaptive space truss structure or a middle sized passenger vehicle. The damper is 208 mm long in its extended position, and 155 mm in fully compressed position. The damper can provide a stroke of ±25 mm. The magnetic field inside the device can be varied externally by monitoring the input current
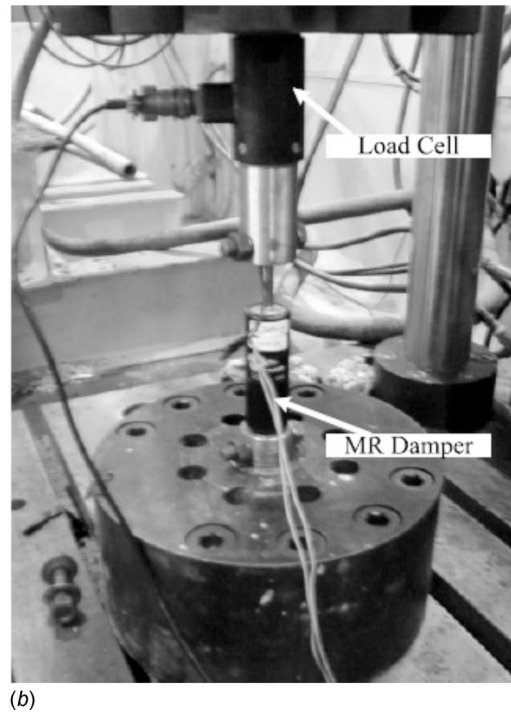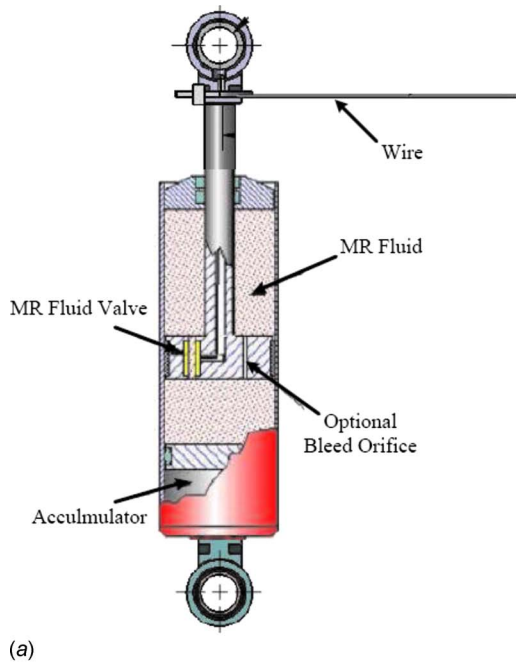
(a)

(b)

Fig. 1   Magnetorheological damper

supplied to the device. The input current can be varied to a maximum of 1 A (continuous supply) and 2 A (intermittent supply). Further details about the damper are available with LORD® Corporation [12].

2.1   Experimental Setup. The MR damper was tested using a computer-controlled Universal Testing Machine, as shown in Fig. 1(b). Figure 1(b) shows the connection of MR damper with the universal testing machine. The lower head is fixed. The upper head is attached to the hydraulic actuator that can move up and down and also incorporates a load cell of 5 kN, allowing the operator to measure the force applied across the damper. The universal testing machine is activated by a hydraulic cylinder; thus it is difficult to carry out high frequency test except for sufficiently small displacement amplitude. A matrix of frequencies (0.1 Hz, 0.25 Hz, 0.50 Hz, 1.0 Hz, 1.5 Hz, 2.0 Hz, 2.5 Hz, and 3.0 Hz), amplitudes (2.5 mm, 5.0 mm, 10.0 mm, 15.0 mm, and 20.0 mm), and current supplies (0.0 A, 0.25 A, 0.50 A, 0.75 A, and 1.0 A) formed the test program.

2.2   Testing. Using the setup depicted in Fig. 1(b), a series of tests was conducted to measure the response of the damper under various combinations of frequencies, amplitude of damper stroke, and current supply. In each test, the hydraulic actuator was driven with a sinusoidal signal with a fixed frequency, and the current applied to the prototype MR damper was held at a constant level. The data were sampled at 128 Hz. The input current is supplied using WonderBox (provided along with MR damper by LORD® Corporation), which converts a voltage to a current supply. Therefore one can monitor either voltage or current synonymously to modify the characteristic of the damper. Since, MR damper directly takes current as an input, this paper develops its algorithm based on current supply to the damper.

Displacement controlled test for the above mentioned frequency, amplitude, and input current has been performed. The velocity of the damper piston has been obtained via derivative of displacement (finite difference), while the resulting force has been measured through the load cell. The MR damper was initially tested without any supply current. Current was then supplied to the coils and the damper tested again. The currents were varied

from 0 A to 1.0 A, and the experimental data including time, displacement, and force have been recorded. All the experiments were carried out at room temperature of 26–32°C.

2.3   Experimental Results and Bouc–Wen Model. The response of the MR damper due to a 0.5 Hz sinusoid with different amplitudes at constant 0.5 A input current is shown in Fig. 2. Bouc–Wen model (see Fig. 3) structure has been considered for a nonlinear least square based model fit of the experimental results. Bouc–Wen model contains six design parameters. For the initial set of run the parameters were assumed free and are allowed to vary with independent variables, namely, input current (i_c), amplitude of stroke (x_a), and frequency (ω) of excitation.

As shown in Fig. 3, force $u(t)$ provided by a MR damper is given by Spencer et al. [13].

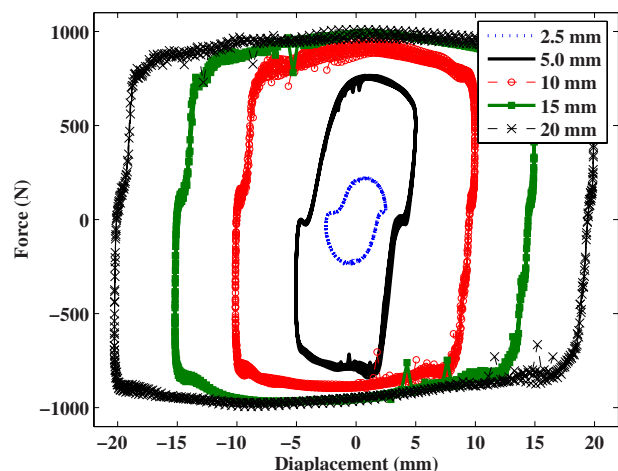$$u(t) = k_0 x(t) + c_0 \dot{x}(t) + \alpha z(t, x)$$

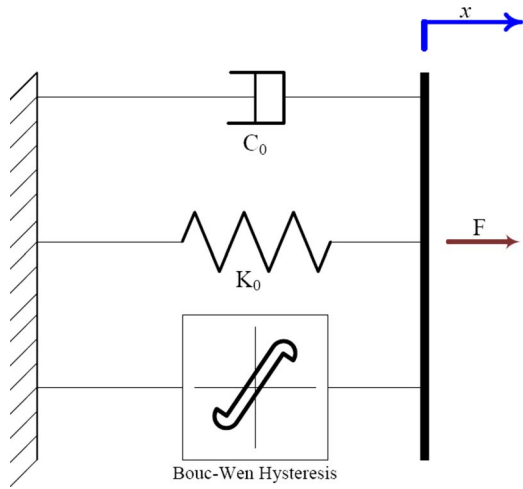**Fig. 2   Force-displacement hysteresis curve (experimental)**

Fig. 3 Bouc–Wen hysteretic model

Table 1 Optimal Bouc–Wen parameters

Parameter	Value
c_1	2.4346
c_4	12.2252
k_1	1.7194
k_4	7.6337
α_1	4.2188
α_4	362.4943
γ	2.85
c_2	−0.2804
c_5	−0.4560
k_2	−0.1244
k_5	−0.2127
α_2	10.0291
α_5	1.0843
β	5.420
c_3	0.0101
c_6	0.0026
k_3	0.0038
k_6	0.0002
α_3	−0.0244
α_6	0.0229
A	12.26

$$\dot{z} = -\gamma|\dot{x}|z|z|^{n-1} - \beta\dot{x}|z|^n + A\dot{x} \tag{1}$$

where x is the displacement at the damper location; z is the evolutionary variable; and γ, β, n, and A are parameters controlling the linearity in the unloading and the smoothness of the transition from the preyield to the postyield region. The functional dependence of the device parameters on the command current i_c is expressed in Eq. (2). The current that changes the magnetic flux in the MR damper is known as commanded current and is different from that of supplied current to the damper (see Eq. (5)).

$$\alpha(\omega, x_a, i_c) = \alpha_a(\omega, x_a) + \alpha_b(\omega, x_a)i_c$$

$$c_0(\omega, x_a, i_c) = c_{0a}(\omega, x_a) + c_{0b}(\omega, x_a)i_c$$

$$k_0(\omega, x_a, i_c) = k_{0a}(\omega, x_a) + k_{0b}(\omega, x_a)i_c \tag{2}$$

The six parameters (c_0, k_0, α, γ, β, and A) are estimated for every single frequency of excitation at a particular amplitude and input current on the basis of minimizing the error between the model-predicted force (u) and the force (Fe) obtained in experiment. The error in the model is represented by the objective function J given by

$$J = \sum_{i=1}^{N} (u_i - Fe_i)^2 \tag{3}$$

where N is the number of points in the experimental data. Optimum values for the six parameters have been obtained using "lsqcurvefit" algorithm available in MATLAB® optimization toolbox for nonlinear curve fitting.

A preliminary set of analysis has been performed to observe the variability of the parameters with independent variables, namely, frequency (ω), amplitude of sinusoid (x_a), and applied current (i_c) for $n = 2$. It is seen that the parameters (γ, β, and A) for the hysteretic behavior of the MR damper show slow change with frequency, amplitude, and input current and therefore are kept constant at their average values for further analysis. Thereafter, the rest of the variables (c_0, k_0, and α) and their dependence on frequency, amplitude, and input current have been evaluated to obtain the optimal values. For the present analysis (keeping in mind the application to seismic structural control) the effects of amplitude of excitation, and input current on the variables have been studied (frequency has been omitted as earthquake excitation frequency is not certain).

3 Modified Bouc–Wen Hysteretic Model

Parameters c_0 and k_0 have been observed to decrease with amplitude of excitation but increase with increase in input current. On the other hand α increases with increase in both x_a and i_c. Bouc–Wen model has been modified for velocity dependence of the c_0 parameter by Yang et al. [10] using an exponential function. Dominguez et al. [21] multiplied the right hand side of Eq. (1) with an exponential function to consider the effect of amplitude of stroke in harmonic analysis of MR dampers. In the present analysis we consider the effect of amplitude of stroke separately for c_0, k_0, and α as a quadratic function of amplitude of stroke (x_a). As shown in Eq. (4), a quadratic in x_a and linear in i_c function has been considered to represent c_0, k_0, and α.

$$c_0 = (c_1 + c_2 x_a + c_3 x_a^2) + (c_4 + c_5 x_a + c_6 x_a^2)i_c$$

$$k_0 = (k_1 + k_2 x_a + k_3 x_a^2) + (k_4 + k_5 x_a + k_6 x_a^2)i_c$$

$$\alpha = (\alpha_1 + \alpha_2 x_a + \alpha_3 x_a^2) + (\alpha_4 + \alpha_5 x_a + \alpha_6 x_a^2)i_c \tag{4}$$

Nonlinear optimization has been carried out to obtain the optimal parameters of the constants (c_1–c_6, k_1–k_6, and α_1–α_6) with the following constraints $c_0(x_a, 0) \geq 0$, $k_0(x_a, 0) \geq 0$, and $\alpha_0(x_a, 0) \geq 0$. Optimization has been carried out for every input current and amplitude of excitation at a frequency of 1 Hz. The optimal parameters obtained as result of optimization are given in Table 1.

The model developed in the present study is an attempt to introduce the amplitude dependency of the Bouc–Wen model. The developed model has a limitation that it is applicable where the excitation is known a priori, which is not the case in many engineering applications. Nevertheless this does not limit the usage of the simple Bouc–Wen model to develop the control strategy based on integral backstepping technique. For the present seismic vibration mitigation application of the MR damper, the damper parameters have been assumed, such that the damper has undergone its maximum displacement (20 mm) and these parameters are given in Table 2.

Figures 4 and 5 show the match between experimental and analytical models. Figure 4 shows the variable amplitude plot of the simulated and experimental results at $i_c = 1$ A, whereas Fig. 5 shows the variable current plot at 10 mm amplitude. Both the results have been simulated at a frequency (ω) of 1 Hz.

Parameter	Value
α_a	1.9504×10^5 N m^{-1}
c_{0a}	8.666×10^2 N s m^{-1}
k_{0a}	7.5140×10^2 N s m^{-1}
η	190 s^{-1}
α_b	3.9334×10^5 N m^{-1} A^{-1}
c_{0b}	4.1452×10^3 N s m^{-1} A^{-1}
k_{0b}	3.4597×10^3 N s m^{-1} A^{-1}
n	2

In addition to the dependence of the parameters on amplitude and current, the resistance and inductance present in the circuit introduce dynamics into this system. This dynamics has been accounted for by the first order filter on the control input given by

$$\dot{i}_c = -\eta(i_c - i_a) \tag{5}$$

where η is the time constant associated with the first order filter and i_a is the current supplied to the current driver.

Equations (1), (4), and (5) show a nonlinear force-supplied current relation. One can determine the force required to suppress the building vibration using feedback techniques, but it is very hard to determine the amount of input current required by the damper to provide that particular force requirement. Therefore, for the clipped optimal strategy, the current input to the damper was switched between 0 A and 2 A (i.e., 0–5 V), based on the comparison of the damper force with the control force required. This method uses current value either 0 A (min) or 2 A (max) and therefore does not make use of full capacity of MR damper. Therefore, there is a need for developing a control scheme, which can directly monitor the current to be set to the damper based on the system feedback as well as provide smooth change in damper input current. Moreover, there has been hardly any exercise reported in literature that considered the supplied-commanded current dynamics into their control algorithms. With these objectives an integrator backstepping based MR damper current control algorithm has been developed and reported in this paper. Section 4 discusses the application of integral backstepping to develop a control strategy where the MR damper current can be monitored directly from system responses.

4 Backstepping Based MR Damper Current Monitoring

4.1 System Model. For the present study we have taken a single degree of freedom (SDOF) spring-dashpot model. The linear dynamics of SDOF systems is given by
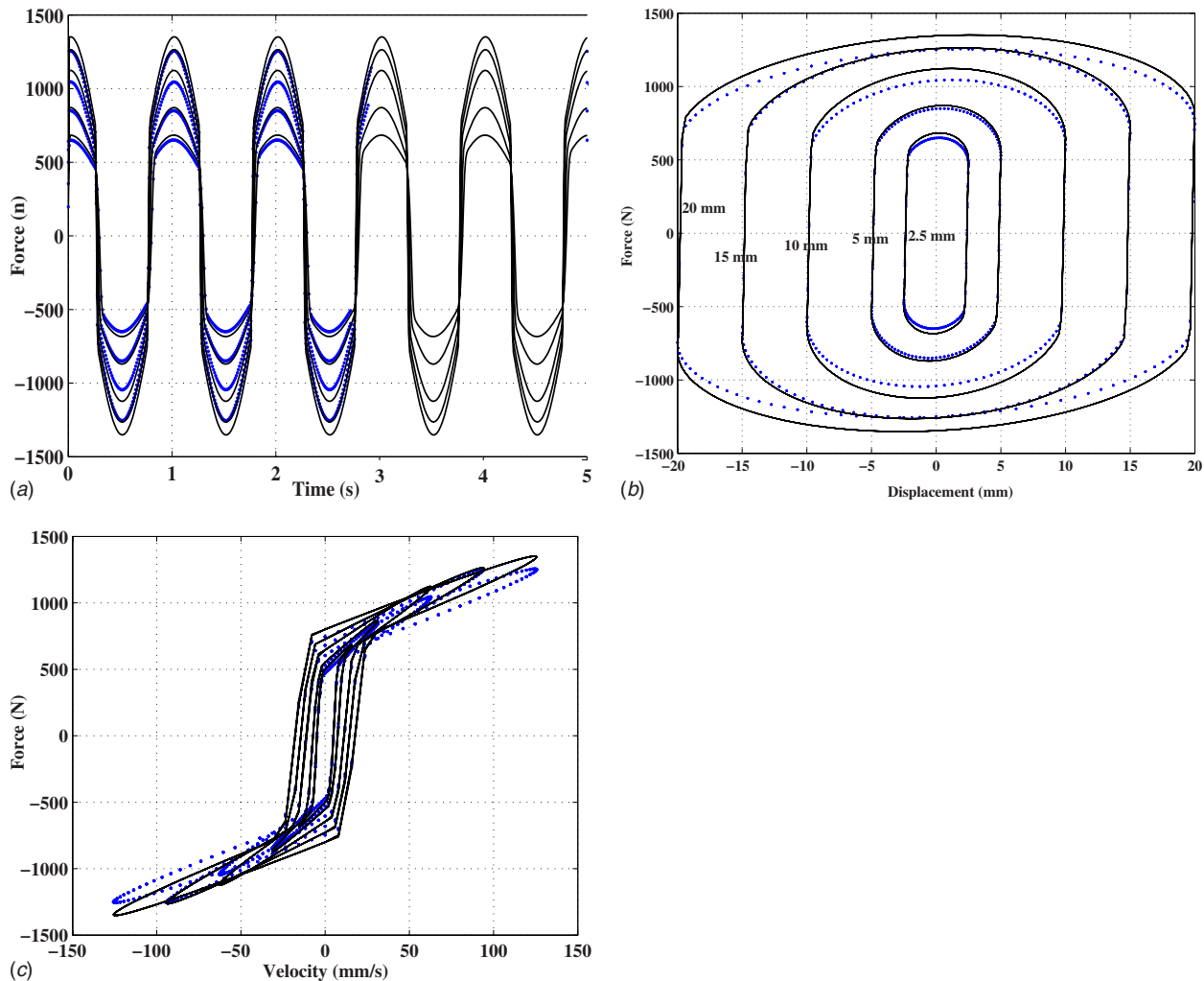

Fig. 4 Comparison of experimental (dotted line) and analytical (solid line) models: variable amplitude (i_c=1.0 A, ω=1.0 Hz)
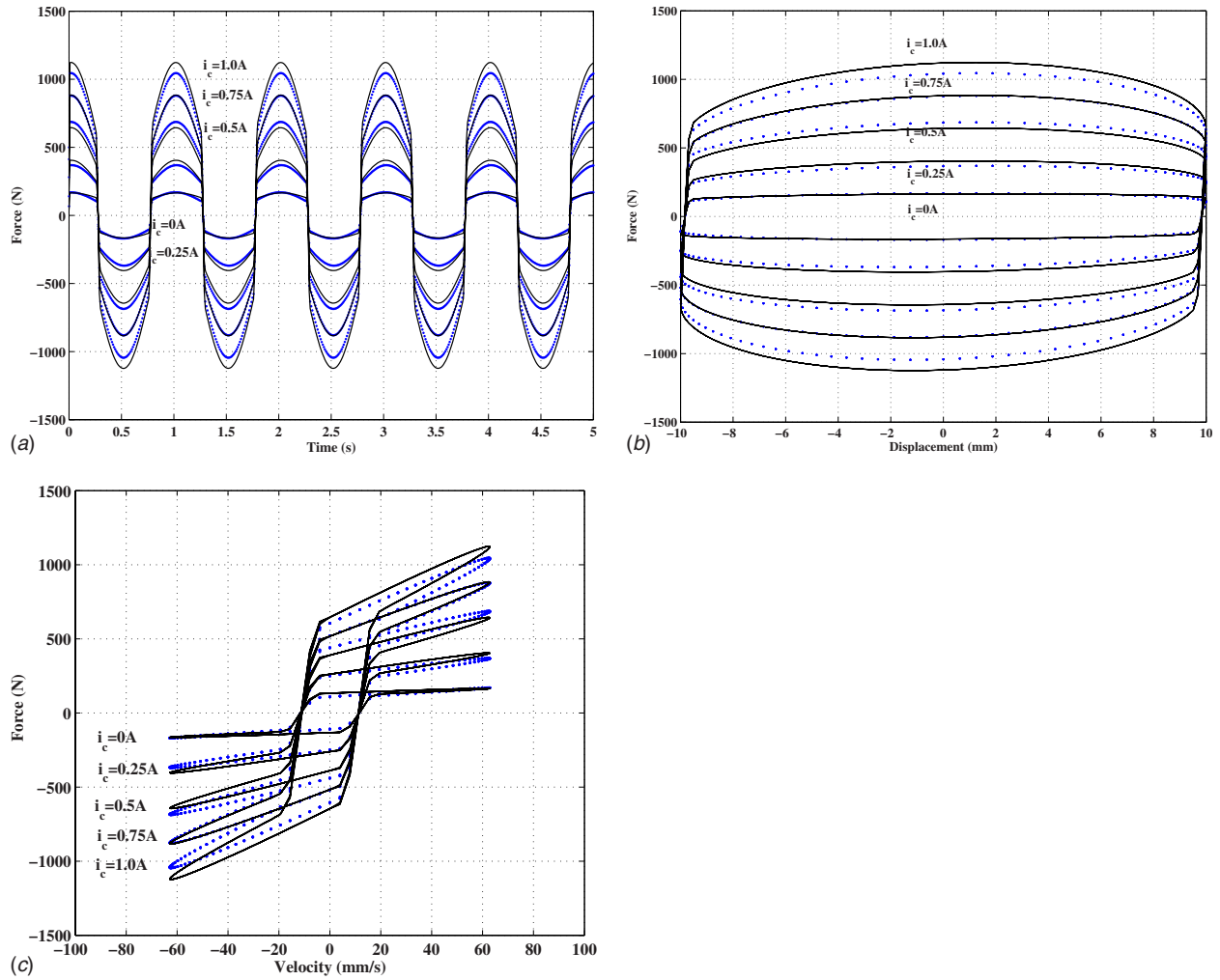
Fig. 5 Comparison of experimental (dotted line) and analytical (solid line) models: variable current (x_a=10 mm, ω=1.0 Hz)

$$m\ddot{x} + c\dot{x} + kx + u(t) = f(t) \qquad (6)$$

where m, c, and k are mass, damping, and stiffness parameters of the SDOF system and (˙) denotes derivative with respect to time (t). $u(t)$ is the damper force and $f(t)$ is the external excitation force. $u(t)$ is added as the system restoring force as the MR damper acts as a passive device in the absence of a driver current.

Since, the maximum stroke of the damper is ± 25 mm and it is advisable to keep a safe passage of 6 mm, we restrict the maximum displacement of the MR damper during operation to ± 20 mm amplitude of displacement. Therefore, the MR damper parameters (c_{0a}, c_{0b}, k_{0a}, k_{0b}, α_a, and α_b) are determined taking x_a =20 mm and constant as defined in Table 1. The values of the MR damper parameters used for simulation of building control are tabulated in Table 2.

Replacing $u(t)$ from Eq. (1) in Eq. (6) and then rewriting the closed loop system dynamics (neglecting the external forcing term) in state space form one gets

$$\dot{x}_1 = x_2$$

$$\dot{x}_2 = -\frac{1}{m}\{(k + k_{0a})x_1 + (c + c_{0a})x_2 + \alpha_a x_3\} - \frac{1}{m}\{k_{0b}x_1 + c_{0b}x_2$$

$$+ \alpha_b x_3\}i_c$$

$$\dot{x}_3 = -\gamma|\dot{x}_2||x_3||x_3|^{n-1} - \beta\dot{x}_2|x_3|^n + A\dot{x}_2$$

$$\dot{i}_c = -\eta(i_c - i_a) \qquad (7)$$

In Eq. (7) the evolutionary variable z (see Eq. (1)) has been replaced with x_3. The variable z is responsible for the hysteretic behavior of the MR damper and it evolutes with time. Therefore it is a hidden variable and therefore has been considered as an additional state variable.

Equation (7) can be represented in the following form:

$$\dot{X} = F_1(t,X) + G_1(t,X)i_c$$

$$\dot{i}_c = F_2(t,X,i_c) + G_2(t,X,i_c)i_a \qquad (8)$$

where X, F_1, G_1, F_2, and G_2 are given in

$$X = [x_1,x_2,x_3]^T$$

$$F_1 = \begin{bmatrix} x_2 \\ -\dfrac{1}{m}\{(k + k_{0a})x_1 + (c + c_{0a})x_2 + \alpha_a x_3\} \\ -\gamma|\dot{x}_2||x_3||x_3|^{n-1} - \beta\dot{x}_2|x_3|^n + A\dot{x}_2 \end{bmatrix}$$

$$G_1 = \left[0, -\frac{1}{m}\{k_{0b}x_1 + c_{0b}x_2 + \alpha_b x_3\}, 0\right]^T$$

$$F_2 = -\eta i_c, \quad G_2 = \eta \tag{9}$$

where ^{T} represents transpose operation.

4.2 Backstepping Controller Design. Equation (8) is a second order strict feedback form of the system given by Eq. (7). To implement integral backstepping on the second part of Eq. (8), we define a dummy variable i_{dum} such that it satisfies the following relation:

$$i_{\text{dum}} = F_2(t,X,i_c) + G_2(t,X,i_c)i_a \tag{10}$$

Equation (10) simplifies the second part of Eq. (8). Therefore, combining Eqs. (10) and (8) we reduce the strict feedback system to integrator backstepping form

$$\dot{X} = F_1(t,X) + G_1(t,X)i_c$$

$$i_c = i_{\text{dum}} \tag{11}$$

The design objective is $X(t) \rightarrow 0$ as $t \rightarrow \infty$. The control law can be synthesized in to two steps. We regard commanded current, i_c, to the damper as the real current driver, first. By choosing the Lyapunov candidate function of the system as $V_1 = 1/2(kx_1^2 + mx_2^2 + qx_3^2)$, we get

$$\dot{V}_1 = \begin{bmatrix} -\{(c+c_{0a})x_2^2 + \gamma q|x_2 x_3|x_3^2\} - \ldots \\ \{k_{0a}x_1 x_2 + (\alpha_a - Aq)x_2 x_3 + q\beta x_2 x_3^3 + (k_{0b}x_1 x_2 + c_{0b}x_2^2 + \alpha_b x_2 x_3)i_c\} \end{bmatrix} \tag{12}$$

The Lyapunov-time-derivative $\dot{V}_1$ should be made negative-definite to get a stable closed loop system. The first term in $\dot{V}_1$, i.e., $\{(c+c_{0a})x_2^2 + \gamma q|x_2 x_3|x_3^2\}$, is free of current variable i_c and is negative-definite $\forall x_2, x_3$. q is positive constant given by α_a/A. Out of many solutions, we select designed commanded current $i_{c_{\text{des}}}$ to be

$$i_{c_{\text{des}}} = \frac{k_d x_1^2 - K_{0a}x_1 x_2 - q\beta x_2 x_3^3}{k_{0b}x_1 x_2 + c_{0b}x_2^2 + \alpha_b x_2 x_3} \tag{13}$$

where $k_d \geq 0$ is a positive constant to be decided by the designer. In the present analysis we have taken $k_d = 1$, which makes $\dot{V}_1 = -\{(c+c_{0a})x_2^2 + \gamma q|x_2 x_3|x_3^2 + k_d x_1^2\} \leq 0 \forall X \neq 0$ in Eq. (12). There can be a numerical stability problem when all $x_1 \rightarrow 0$, $x_2 \rightarrow 0$, and $x_3 \rightarrow 0$ simultaneously. Therefore, we set a tolerance (tol $= 10^{-4}$ for all the state variables) below which the damper input current is kept at zero. Nevertheless, i_c is a state variable and perfect tracking to $i_{c_{\text{des}}}$ is desired. Therefore, we define an error variable e (given in Eq. (14)) as the target error of the designed variable.

$$e = i_c - i_{c_{\text{des}}} \tag{14}$$

The error dynamics is given by

$$\dot{e} = \dot{i}_c - \dot{i}_{c_{\text{des}}} = i_{\text{dum}} - i_{c_{\text{des}},X}\dot{X} \tag{15}$$

where $i_{c_{\text{des}},X}$ is the derivative of $i_{c_{\text{des}}}$ with respect to state X. A second Lyapunov function has been chosen as $V_2 = V_1 + \frac{1}{2}e^2$ with the current variable i_{dum} as given in Eq. (16). The implication of considering a second Lyapunov function is to minimize the error between desired and obtained commanded currents along with the system dynamics. This second Lyapunov function allows to consider the dynamics of the supplied-commanded current in the algorithm (this was one of our goals). One can show that the system defined in Eq. (11) becomes asymptotically stable (see Refs. [29,30]).

$$i_{\text{dum}} = i_{c_{\text{des}},X}[F_1(t,X) + G_1(t,X)i_c] - V_{1,X} \cdot G_1(t,X) - K(i_c - i_{c_{\text{des}}}) \tag{16}$$

with F_1 and G_1 defined in Eq. (9) and $K > 0$ is any constant to be decided by the designer. For our analysis $K = 1$ has been taken.

5 Numerical Example

A three story base isolated building model (shown in Fig. 6) has been considered for the numerical simulation study. In Fig. 6, x_g

and u_b are the ground displacement (seismic motion) and the base displacement, respectively. The floor displacements with respect to the base are represented by u_1, u_2, and u_3 for the first, second, and third floors, respectively. The mass, stiffness, and damping of the base are given by m_b (40 kg), k_b (4.32 N/m), and c_b (2% of critical), respectively. Similarly, the ith floor mass, stiffness, and damping ($i = 1, 2, 3$) are represented by m_i, k_i, and c_i, respectively.

5.1 Base Isolated Building Model. The superstructure is modeled as a linear shear frame building model, i.e., the floor slabs and the base slab are assumed to be rigid in plane. The MR dampers are assumed to be attached at the base of the building to minimize base displacement. The equations of motion for the elastic superstructure are expressed in the following form:

$$M_s\ddot{U} + C_s\dot{U} + K_sU = -M_sR(\ddot{x}_g + \ddot{u}_b) \tag{17}$$

in which M_s, C_s, and K_s are the superstructure mass matrix, damping matrix, and stiffness matrix, respectively (given in Eq. (18)).
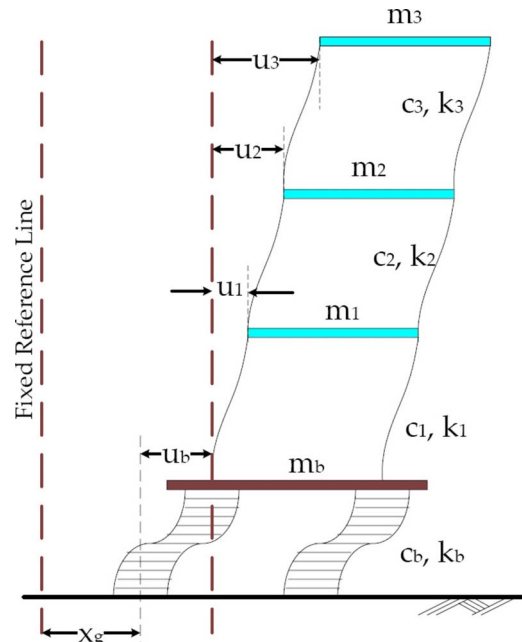

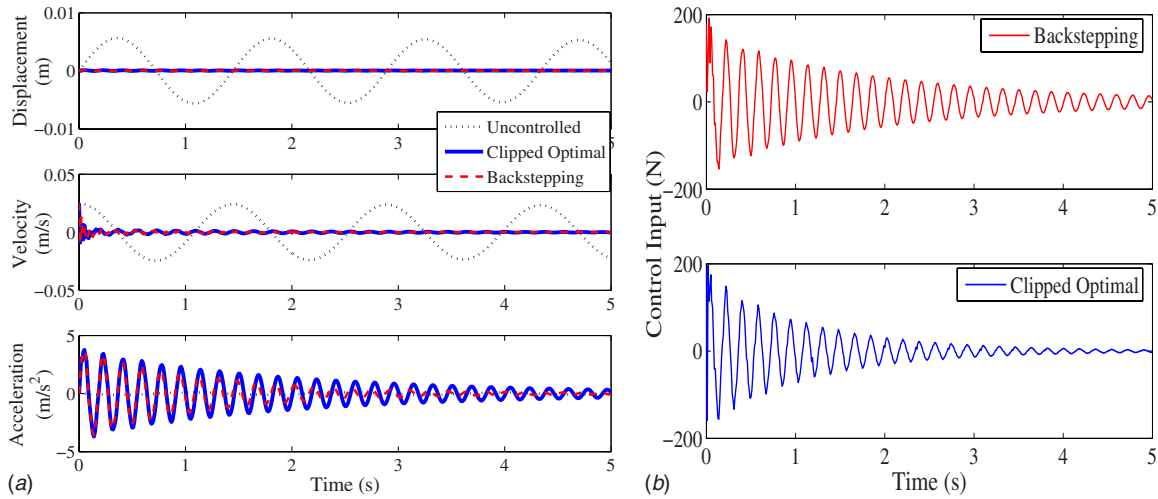**Fig. 6 Base isolated three story building model**

Fig. 7 Impulse force analysis: (*a*) uncontrolled and uncontrolled responses, and (*b*) control force input

$R=[111]^T$ is the matrix of earthquake influence coefficients. Furthermore, $\ddot{U}$, $\dot{U}$, and $U=[u_1 u_2 u_3]^T$ represent the floor acceleration, velocity, and displacement vectors relative to the base, $\ddot{u}_b$ is the base accelerations relative to the ground, and $\ddot{x}_g$ is the ground accelerations.

$$M_a = \begin{bmatrix} 62.76 & 0 & 0 \\ 0 & 64.20 & 0 \\ 0 & 0 & 59.40 \end{bmatrix} \text{ kg},$$

$$C_a = \begin{bmatrix} 522.75 & -222.75 & 0 \\ -222.75 & 232.75 & -10.00 \\ 0 & -10.00 & 10.00 \end{bmatrix} \text{ N s/m}$$

$$K_a = \begin{bmatrix} 1.0394 & -0.7338 & 0 \\ -0.7338 & 1.4931 & -0.7593 \\ 0 & -0.7593 & 0.7593 \end{bmatrix} \times 10^6 \text{ N/m} \quad (18)$$

The equation of motion for the base is given by [31,32]

$$R^T M_s [\ddot{U} + R(\ddot{x}_g + \ddot{u}_b)] + m_b(\ddot{x}_g + \ddot{u}_b) + c_b \dot{u}_b + k_b u_b + u(t) = 0 \quad (19)$$

The MR damper control force is given by $u(t)$.

Since the superstructure in a base isolated structure behaves as a rigid block, it can be modeled as a SDOF system [32]. In the present analysis the integral backstepping based MR damper monitoring has been formulated assuming the structure to be a SDOF system. The mass of the structures is assumed to be concentrated at the base. Therefore, in Eq. (7), we have substituted $m=m_b+\Sigma_{i=1}^3 m_i$, $x_1=u_b$, and $x_2=\dot{u}_b$.

The MR damper parameters taken for the present analysis are given in Table 2. The maximum input current allowed for the damper is 2 A. The MR damper force increases with the increase in current supply. The maximum force the damper can provide is ± 2250 N.

Numerical simulation results have been presented for an impulsive force on the system and under base excitation. Comparison with widely used on-off clipped-optimal control strategy has been provided. First we present the control of impulsive force response, where impulsive force has been simulated by setting the system with an initial velocity [31] at the base. Second the performance of the proposed MR damper current monitoring technique has been shown by controlling the base isolated system under a set of seismic ground motion.

5.2 Impulse Response Test. For the simulation of impulse response, external force $f(t)$ in the system (6) has been taken to be zero and the initial conditions have been taken as $U(0)=0$, $u_b=0$, $\dot{U}(0)=0$, and $\dot{u}_b=1/m_b$ m/s, i.e., $x_1=0$, $x_2=0.025$, and $x_3=0$. The goal is to bring the system dynamics to zero condition. The simulation has been run for 5 s as the controlled responses are seen to achieve the goal well before 10 s.

Figure 7(*a*) shows the time history of the uncontrolled and controlled system responses at the base of the structure. The uncontrolled and controlled displacements, velocity, and acceleration responses for both backstepping and on-off clipped-optimal cases have been shown together for better comparison. The uncontrolled system responses continue even after 5 s with decaying amplitude (due to viscous damping). The controlled responses are seen to die down well within 5 s. It has been observed from the numerical simulation that the displacement-time history took 2.2 s and 5 s to reach 10% of maximum displacement for backstepping control and on-off clipped-optimal control cases, respectively. In case of velocity-time history overshoot of 0.01 m/s has been observed for both the control cases.

With the use of MR damper the peak displacement of the system has been reduced from 5.7×10^{-3} m in uncontrolled case to 1.145×10^{-3} m in backstepping case and 1.449×10^{-3} m in on-off clipped-optimal case. The peak acceleration has gone up from 0.1168 m/s^2 to 3.6725 m/s^2 and 3.7846 m/s^2 in backstepping and clipped-optimal cases, respectively. The velocity response at the base is also seen to be reduced using MR damper.

The force required and current supplied to the MR damper for both backstepping and on-off clipped-optimal cases have been shown in Figs. 7(*b*) and 8. It is evident from Fig. 7(*b*) that the supplied control force to the system is similar in both the control strategies. Figure 8 shows the current supplied to MR damper in both backstepping and on-off clipped-optimal cases.

It can be noticed that the current input in the backstepping control case does not jump as in the case of clipped-optimal case. The maximum current required by the MR damper in backstepping control case is only 0.005 A, whereas clipped-optimal provides full 2 A current supply. Therefore in the present situation the passive-off (MR damper with 0 A current) case will be sufficient to provide similar control efficiency. As shown in Fig. 8 the voltage in backstepping case dies down exponentially as the system reaches its goal. The objective of the present technique is to provide a MR damper current monitoring technique such that it gradually changes the current input to the MR damper unlike clipped-optimal strategy where the voltage (and therefore current)
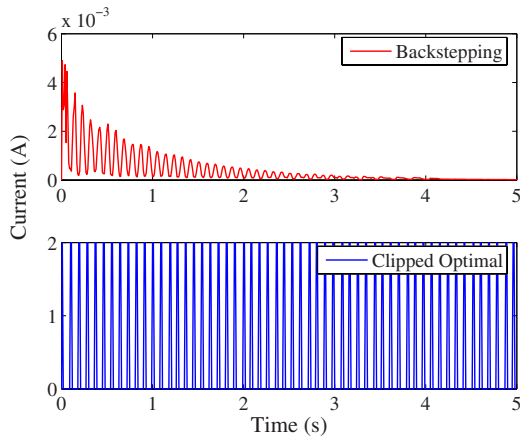
Fig. 8   Base isolated three story building model

jumps between 0 and its maximum allowed value (in the present case it is 5 V or 2 A) depending on the force feedback from the damper [5]. The second objective is to access all available current values of the damper, which was not possible in clipped-optimal case (since the input supply jumps between minimum and maximum values). From Fig. 8 one can see that the maximum current supplied to the MR damper is 0.005 A. Therefore the system never needed the maximum 2 A (and therefore 5 V) to be supplied. Therefore the objectives of the present study are met satisfactorily.

5.3   Seismic Analysis. Base isolated structures behave as a rigid mass over the base under seismic ground motion [31]. Therefore SDOF models provide good approximation to these systems for quick calculation under seismic excitations [31]. Under near field pulse type seismic motion where velocity components are much higher these base isolated structures undergo huge displacements. To minimize the displacements base isolated structures are often clubbed with MR damper as a hybrid mechanism [26]. A new methodology to monitor the MR damper current for control of structures under seismic motions has been proposed. Four earthquake records have been considered for the numerical simu-

lation. Details of the results obtained from simulation with North Palm Spring seismic motion data have been provided and results for other earthquake records have been tabulated in Tables 3 and 4.

For seismic analysis the initial conditions have been taken as $x_1=0$, $x_2=0$, and $x_3=0$ and the external force $f(t)$ has been replaced with $m\ddot{x}_g$ where $\ddot{x}_g$ is the seismic ground acceleration [31].

Figure 9 shows the uncontrolled and controlled responses obtained through simulation with North Palm Spring ground motion data. Figure 9 contains both uncontrolled and controlled time histories (both backstepping and on-off clipped-optimal strategies) for better comparison. Figure 9(a) shows the displacement-time histories. It is evident from Fig. 9(a) that the controllers are effective in reducing the displacement in the structure. Numerically the peak displacement has been reduced to 2% of its value at uncontrolled case. Performance efficiencies of 62% and 55% have been observed in reducing peak velocity using backstepping and clipped-optimal control strategies, respectively, which is also evident from Fig. 9(b). On the other hand the peak acceleration has been reduced by 5% in backstepping control but increased by 2.7% in clipped-optimal control case. The acceleration time histories have been compared in Fig. 9(c). One can notice a sudden rise in base acceleration in clipped-optimal case. This sudden jerk is attributed to the sudden rise in MR damper input current. This is also evident from MR damper input control force (Fig. 9(d)). The current inputs to the MR damper for both backstepping and on-off clipped-optimal control cases have been shown in Fig. 9(d).

Simulation results for other seismic records have been reported in Tables 3 and 4. The maximum responses have been provided in Table 3, whereas the corresponding norms are given in Table 4. The controlled responses with backstepping (IB) and clipped-optimal (CO) strategies are provided together for better comparison. The controlled responses have been normalized with respect to the corresponding values in uncontrolled case. "unc" is short for uncontrolled responses and "cont" represents controlled responses. One can notice from Table 3 that the overall performance of backstepping based control algorithm is slightly better than on-off clipped-optimal strategy. The norm responses (see Table 4) for backstepping based strategy are slightly higher than clipped-optimal at the base and the first floor, but, at the higher floor the

Table 3   Performance with seismic records for peak values of variables

| | | Chi-Chi | | Capemend | | Elcentro | | Npalm Spring | |
| | | Earthquake records | | | | | | | |
PI	**Floor**[a]	IB	CO	IB	CO	IB	CO	IB	CO
	BI	0.019	0.020	0.029	0.03	0.084	0.108	0.028	0.029
	FF	0.196	0.245	0.439	0.627	0.942	1.066	0.249	0.392
	SF	0.206	0.258	0.459	0.654	0.939	1.117	0.251	0.415
U_{cont}/U_{unc}	TF	0.211	0.266	0.473	0.664	0.937	1.139	0.257	0.429
	BI	0.038	0.045	0.059	0.059	0.221	0.243	0.054	0.068
	FF	1.796	2.109	3.864	4.239	8.603	9.968	2.518	3.477
	SF	1.789	2.051	3.620	4.543	7.654	9.975	2.159	4.135
$\dot{U}_{cont}/\dot{U}_{unc}$	TF	1.839	2.069	4.310	5.271	7.293	11.22	2.204	4.184
	BI	0.957	1.271	2.127	2.894	4.065	5.610	1.122	1.951
	FF	67.25	92.07	163.81	218.45	184.99	248.40	81.22	135.89
	SF	60.86	79.20	143.33	198.69	126.71	169.42	69.77	123.04
$\ddot{U}_{cont}/\ddot{U}_{unc}$	TF	61.06	77.42	141.29	188.48	112.09	152.76	77.06	125.85
$u(t)/m$	-	1.315	2.079	1.255	1.886	2.675	2.837	1.465	3.504
i_a	-	0.053	2.0	0.161	2.0	0.207	2.0	0.139	2.0

[a]FF=First floor, SF=Second floor, and TF=Third floor.

Table 4 Performance with seismic records for L_2 norm of variables

Variables		Earthquake records							
		Chi-Chi		Capemend		Elcentro		Npalm Spring	
PI	Floor[a]	IB	CO	IB	CO	IB	CO	IB	CO
	BI	0.006	0.005	0.023	0.046	0.035	0.038	0.015	0.015
	FF	0.101	0.096	0.207	0.202	0.567	0.577	0.148	0.144
	SF	0.102	0.097	0.209	0.204	0.575	0.587	0.149	0.146
$\|U_{cont}\|/\|U_{unc}\|$	TF	0.102	0.098	0.211	0.206	0.580	0.594	0.150	0.148
	BI	0.005	0.005	0.010	0.009	0.059	0.057	0.015	0.015
	FF	0.542	0.509	1.314	1.288	3.666	4.330	0.882	0.929
	SF	0.553	0.518	1.339	1.312	3.765	4.363	0.904	0.959
$\|\dot{U}_{cont}\|/\|\dot{U}_{unc}\|$	TF	0.562	0.530	1.364	1.355	3.875	4.541	0.923	0.991
	BI	0.48	0.45	0.98	0.99	2.67	2.73	0.70	0.69
	FF	45.56	43.70	94.61	94.78	207.48	212.99	66.54	65.21
	SF	36.93	35.34	77.08	76.87	161.78	165.82	54.11	53.13
$\|\ddot{U}_{cont}\|/\|\ddot{U}20g_{unc}\|$	TF	34.46	32.97	72.19	72.00	146.47	150.56	50.59	49.81

[a]FF=First floor, SF=Second floor, and TF=Third floor.

performance of backstepping is better than clipped-optimal control strategy.

The maximum force provided by the damper in backstepping case is always in lower than clipped-optimal strategy. The maximum input current supply to the damper never reaches to its maximum at 2 A. The maximum control force supplied by the MR damper has been normalized with respect to the total mass of the structure. It is evident from Table 3 that the MR damper is effective in reducing the responses below 5% of the uncontrolled responses in many of the earthquake simulations. In all the cases, namely, impulsive force response and earthquake ground motion,

the proposed backstepping based MR damper input current monitoring has been shown to suppress the uncontrolled structural responses effectively in comparison to on-off clipped-optimal strategy.

6 Conclusion

Deployment of MR dampers to a system put challenges in modeling the damper characteristic as well as in developing proper control strategy to effectively use the damper capacity. The present paper proposes an amplitude and current dependent modi-
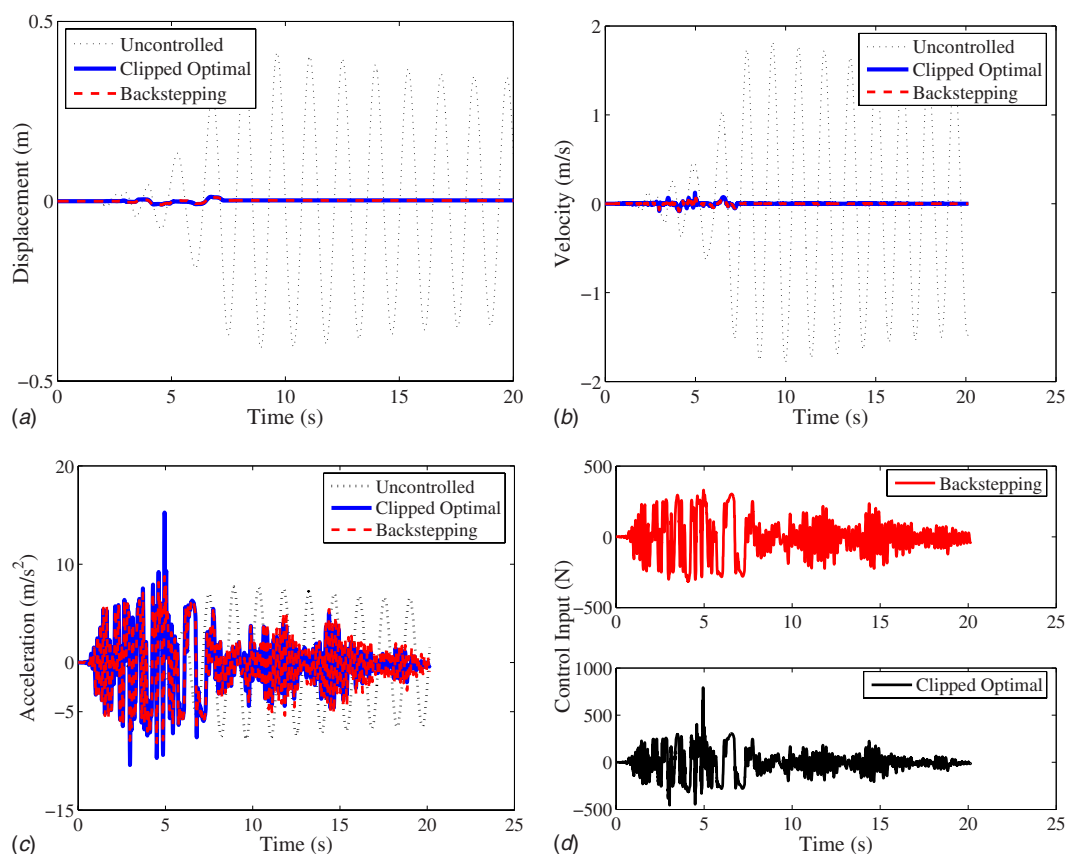

Fig. 9 Seismic analysis: uncontrolled and controlled responses (North Palm Spring, 1994)

fied Bouc–Wen model to characterize the nonlinear hysteretic behavior of the MR damper. Based on the proposed model a new nonlinear control strategy has been developed, which overcomes the existing drawbacks of clipped-optimal type control strategy. The proposed method not only uses the full current range available for control but also changes the current gradually and thereby avoids sudden jerks to the system. Furthermore, the present controller considers the commanded to supplied current dynamics, which is absent in any control algorithm available in literature. Displacement and velocity at the damper location are needed for feedback. The technique is stable in Lyapunov sense and has been shown to control structural responses effectively under impulsive force as well as due to earthquake ground motions.

References

[1] Soong, T. T., and Dargush, G. F., 1997, *Passive Energy Dissipation Systems in Structural Engineering*, Wiley, England.
[2] Soong, T., and Spencer, B., 2002, "Supplemental Energy Dissipation: State of the Art and State of the Practice," Eng. Struct., **24**, pp. 243–259.
[3] Ginder, J. M., Davis, L., and Elie, L., 1996, "Rheology of Magnetorheological Fluids: Models and Measurements," Int. J. Mod. Phys. B, **10**, pp. 3293–3303.
[4] Dyke, S., and Spencer, B., 1997, "A Comparison of Semi-Active Control Strategies for the MR Damper," Proceedings of the IASTED International Conference, Intelligent Information Systems, Bahamas.
[5] Dyke, S., Spencer, B., Sain, M., and Carlson, J., 1996, "Modeling and Control of Magnetorheological Dampers for Seismic Response Reduction," Smart Mater. Struct., **5**, pp. 565–575.
[6] Yi, K., and Song, B. S., 1999, "A New Adaptive Sky-Hook Control of Vehicle Semi-Active Suspensions," Proc. Inst. Mech. Eng., Part D (J. Automob. Eng.), **213**(3), pp. 293–303.
[7] Zhou, L., Chang, C., and Wang, L., 2003, "Adaptive Fuzzy Control for Nonlinear Building Magnetorheological Damper System," J. Struct. Eng., **129**, pp. 905–913.
[8] Liu, M., Song, G., and Li, H., 2007, "Non-Model-Based Semi-Active Vibration Suppression of Stay Cables Using Magneto-Rheological Fluid Dampers," Smart Mater. Struct., **16**, pp. 1447–1452.
[9] Karnopp, D., Crosby, M., and Harwood, R., 1974, "Vibration Control Using Semi-Active Force Generators," ASME J. Eng. Ind., **96**, pp. 619–626.
[10] Yang, G., Spencer, B., Jung, H. H., and Carlson, J. D. J., 2004, "Dynamic Modeling of Large-Scale Magnetorheological Damper Systems for Civil Engineering Applications," J. Eng. Mech., **130**, pp. 1107–1114.
[11] Wereley, N., and Pang, L., 1998, "Nondimensional Analysis of Semi-Active Electrorheological and Magnetorheological Dampers Using Approximate Parallel Plate Models," Smart Mater. Struct., **7**, pp. 732–743.
[12] 2007, LORD®, LORD Technical Data: RD-1005 Damper, LORD Corporation, URL: http://www.lordfulfillment.com/upload/DS7017.pdf.
[13] Spencer, B. F., Jr., Dyke, S. J., Sain, M. K., and Carlson, J. D., 1997, "Phenomenological Model for Magnetorheological Dampers," J. Eng. Mech., **123**,

[14] Ehrgott, R., and Masri, S., 1992, "Modeling the Oscillatory Dynamic Behavior of Electrorheological Materials in Shear," Smart Mater. Struct., **1**, pp. 275–285.
[15] Makris, N., and Dargush, G., 1994, "Generalized Boundary Element Formulation for Dynamic Analysis of Viscoelastic System," Proceedings of the First World Conference on Structural Control, 3–5 August 1994, Pasadena CA, pp. 73–81.
[16] Kamath, G., Hurt, H., and Wereley, N., 1996, "Analysis and Testing of Bingham Plastic Behavior in Semi-Active Electrorheological Fluid Dampers," Smart Mater. Struct., **5**, pp. 576–590.
[17] Kamath, G., and Wereley, N., 1997, "Nonlinear Viscoelastic-Plastic Mechanisms Based Model of an Electrorheological Damper," J. Guid. Control Dyn., **20**, pp. 1125–1132.
[18] Li, W. H., Yao, G. Z., Chen, G., Yeo, S. H., and Yap, F. F., 2000, "Testing and Steady State Modeling of a Linear MR Damper Under Sinusoidal Loading," Smart Mater. Struct., **9**, pp. 95–102.
[19] Vavreck, A. N., 2002, "Single-Stage Magnetorheological Damper Parameter Estimation," Smart Mater. Struct., **11**, pp. 596–598.
[20] Dominguez, A., Sedaghati, R., and Stiharu, I., 2004, "Modelling the Hysteresis Phenomenon of Magnetorheological Dampers," Smart Mater. Struct., **13**, pp. 1351–1361.
[21] Dominguez, A., Sedaghati, R., and Stiharu, I., 2006, "A New Dynamic Hysteresis Model for Magnetorheological Dampers," Smart Mater. Struct., **15**, pp. 1179–1189.
[22] Feng, Q., and Shinozuka, M., 1990, "Use of a Variable Damper for Hybrid Control of Bridge Response Under Earthquake," *Proceedings of the U.S. National Workshop on Structural Control Research*, edited by G. Housner and S. Masri, University of Southern California, Los Angeles, CA, pp. 107–112.
[23] Leitmann, G., 1994, "Semi-Active Control for Vibration Attenuation," J. Intell. Mater. Syst. Struct., **5**, pp. 841–846.
[24] Inaudi, J., 1997, "Modulated Homogeneous Friction: A Semi-Active Damping Strategy," Earthquake Eng. Struct. Dyn., **26**, pp. 361–376.
[25] Jansen, L., and Dyke, S., 2000, "Semi-Active Control Strategies for MR Dampers: Comparative Study," J. Eng. Mech., **126**, pp. 795–803.
[26] Nagarajaiah, S., and Narasimhan, S., 2006, "Smart Base Isolated Benchmark Building Part II: Phase I Sample Controllers for Linear Isolation System," Struct. Control Health Monit., **13**, pp. 589–604.
[27] Ali, S. F., and Ramaswamy, A., 2008, "GA Optimized FLC Driven Semi-Active Control for Phase II Smart Nonlinear Base Isolated Benchmark Building," Struct. Control Health Monit., **15**, pp. 797–820.
[28] Ni, Y., Chen, Y., Ko, J., and Cao, D., 2002, "Neuro-Control of Cable Vibration Using Semi-Active Magneto-Rheological Dampers," Eng. Struct., **24**, pp. 295–307.
[29] Kritic, M., Kanellakopoulos, I., and Kokotovic, P., 1995, *Nonlinear and Adaptive Control Design*, Wiley, New York.
[30] Marquez, H., 2003, *Nonlinear Control Systems Analysis and Design*, Wiley Interscience, Hoboken, New Jersey.
[31] Chopra, A., 2005, *Dynamics of Structures: Theory and Application to Earthquake Engineering*, Pearson Education, New Delhi, India.
[32] Naeim, F., and Kelly, J., 1999, *Design of Seismic Isolated Structures: From Theory to Practice*, Wiley, New York.